

## Chronic Pulmonary Artery Pressure Elevation Is Insufficient to Explain Right Heart Failure

Harm J. Bogaard, MD, PhD\*; Ramesh Natarajan, PhD\*; Scott C. Henderson, PhD;  
Carlin S. Long, MD; Donatas Kraskauskas, DVM; Lisa Smithson, BSc; Ramzi Ockaili, PhD;  
Joe M. McCord, PhD; Norbert F. Voelkel, MD

**Background**—The most important determinant of longevity in pulmonary arterial hypertension is right ventricular (RV) function, but in contrast to experimental work elucidating the pathobiology of left ventricular failure, there is a paucity of data on the cellular and molecular mechanisms of RV failure.

**Methods and Results**—A mechanical animal model of chronic progressive RV pressure overload (pulmonary artery banding, not associated with structural alterations of the lung circulation) was compared with an established model of angioproliferative pulmonary hypertension associated with fatal RV failure. Isolated RV pressure overload induced RV hypertrophy without failure, whereas in the context of angioproliferative pulmonary hypertension, RV failure developed that was associated with myocardial apoptosis, fibrosis, a decreased RV capillary density, and a decreased vascular endothelial growth factor mRNA and protein expression despite increased nuclear stabilization of hypoxia-induced factor-1 $\alpha$ . Induction of myocardial nuclear factor E2-related factor 2 and heme-oxygenase 1 with a dietary supplement (Protandim) prevented fibrosis and capillary loss and preserved RV function despite continuing pressure overload.

**Conclusion**—These data brought into question the commonly held concept that RV failure associated with pulmonary hypertension is due strictly to the increased RV afterload. (*Circulation*. 2009;120:1951-1960.)

**Key Words:** angiogenesis ■ heart failure ■ microcirculation ■ pressure ■ pulmonary heart disease

Pulmonary hypertension and subsequent right heart failure are increasingly being identified as worldwide problems affecting patients with highly prevalent diseases such as schistosomiasis, sickle cell disease, HIV infection, chronic obstructive pulmonary disease, and chronic left heart failure.<sup>1</sup> Right ventricular (RV) function is the most important determinant of longevity in patients with pulmonary arterial hypertension (PAH), a form of pulmonary hypertension characterized by typical vascular lesions in small pulmonary arteries.<sup>2</sup> Pulmonary hypertension and RV failure are strong predictors of mortality in patients with left ventricular (LV) failure<sup>3,4</sup> and chronic obstructive pulmonary disease.<sup>5</sup> The various structural, functional, and developmental differences that exist between the RV and LV caution us to assume that RV failure is mechanistically not different from LV failure.<sup>6</sup>

### Clinical Perspective on p 1960

Because neither a persistent reversal of pulmonary vascular changes nor a lasting reduction of the pulmonary artery pressure can be accomplished in PAH patients by currently

available vasodilator therapies, a specific cardioprotective treatment strategy that improves RV function despite elevated RV afterload may improve the quality of life and survival of PAH patients. Clinical observation and experimental evidence suggest that the mechanical stress of an elevated pulmonary artery pressure is not the only reason for PAH-associated RV failure. RV pressure overload associated with pulmonary artery stenosis carries a much better prognosis than PAH.<sup>7</sup> Progressive pulmonary stenosis induced by pulmonary artery banding (PAB) in rats is not associated with RV failure,<sup>8</sup> but animal models of peripheral pulmonary vascular disease are, despite a similar degree of pressure overload.<sup>9</sup> Pressure-independent components of pulmonary vascular disease may contribute to the development of RV failure in PAH. We hypothesize that progressive pressure overload per se is insufficient to explain RV failure in PAH.

Here, we investigate the relevance to PAH-associated RV failure of 2 mechanisms that play a role in pressure overload-induced LV failure: myocardial fibrosis<sup>10</sup> and a decreased myocardial capillary density (microvascular rarefaction).<sup>11</sup>

Received March 23, 2009; accepted September 1, 2009.

From the Divisions of Pulmonary and Critical Care (H.J.B., R.N., D.K., L.S., N.F.V.) and Cardiology (R.O.), Department of Medicine, and Department of Anatomy and Neurobiology (S.C.H.), Virginia Commonwealth University, Richmond; Department of Pulmonary Medicine, VU University Medical Center, Amsterdam, the Netherlands (H.J.B.); and Divisions of Cardiology (C.S.L.) and Pulmonary Sciences (J.M.M.), Department of Medicine, University of Colorado at Denver and Health Sciences Center, Aurora.

\*Drs Bogaard and Natarajan contributed equally to this work.

The online-only Data Supplement is available with this article at <http://circ.ahajournals.org/cgi/content/full/CIRCULATIONAHA.109.883843/DC1>.

Correspondence to Norbert F. Voelkel, MD, Department of Medicine, Virginia Commonwealth University, 1220 E Broad St, Richmond, VA 23298-0281. E-mail [nvoelkel@mcvh-vcu.edu](mailto:nvoelkel@mcvh-vcu.edu)

© 2009 American Heart Association, Inc.

*Circulation* is available at <http://circ.ahajournals.org>

DOI: 10.1161/CIRCULATIONAHA.109.883843

**Table. Rat Characteristics, Ultrasound Findings, and Hemodynamics in Control Rats, Rats 6 Weeks After PAB, and Rats 6 Weeks After SU5416 and Hypoxic Exposure**

	BW, g	RV, mg	RV/LV+S	TAPSE, mm	HR, bpm	SV, $\mu$ L	CO, mL/min
Controls (n=6)	362 $\pm$ 14	202 $\pm$ 19	0.24 $\pm$ 0.02	3.5 $\pm$ 0.2	312 $\pm$ 15	206 $\pm$ 46	62.2 $\pm$ 5.2
PAB (n=8)	357 $\pm$ 25*	451 $\pm$ 71††	0.52 $\pm$ 0.07††	2.6 $\pm$ 0.7§‡	297 $\pm$ 12	199 $\pm$ 25	59.7 $\pm$ 7.1
SuHx (n=8)	324 $\pm$ 34†	663 $\pm$ 146†	0.76 $\pm$ 0.17†	1.5 $\pm$ 0.5†	292 $\pm$ 15	127 $\pm$ 22#	37.3 $\pm$ 6.3#

BW indicates body weight; RV, RV weight; LV, LV weight; S, septal weight; TAPSE, tricuspid annular plane systolic excursion; HR, heart rate; SV, stroke volume; and CO, cardiac output. Hearts were harvested at 13 to 14 weeks of age. Values are mean $\pm$ SD.

\* $P$ <0.05 versus SuHx; † $P$ <0.0001 versus controls; ‡ $P$ <0.0001 versus SuHx; § $P$ <0.05 versus controls; || $P$ <0.01 vs SuHx; # $P$ <0.01 versus controls.

RV fibrosis has been documented in RV endomyocardial biopsies of PAH patients,<sup>12</sup> and RV ischemia has been described in PAH patients with normal coronary arteries.<sup>13</sup> Whereas RV ischemia is usually attributed to systemic hypotension, enhanced systolic compression of coronary vessels, and increased oxygen demand resulting from elevated wall stress, loss of RV microvessels may play an additional role.<sup>14</sup> Because angiogenesis is necessary to support hypertrophy induced by pressure overload, insufficient hypoxia-induced factor-1 $\alpha$  (HIF-1 $\alpha$ ) protein stabilization or an insufficient upregulation of vascular endothelial growth factor (VEGF) in response to HIF-1 $\alpha$  could lead to capillary growth lagging behind cardiomyocyte growth and hence a decrease in capillary density. The former has been shown in LV pressure overload in mice, and the loss of capillaries has been suggested to contribute to LV failure.<sup>15</sup> Here, we show evidence for dysfunctional HIF-1 $\alpha$ /VEGF signaling in PAH-associated RV failure—defective VEGF protein and receptor transcription associated with oxidative stress—and provide evidence that pressure overload per se is insufficient as a cause of RV failure.

## Methods

RV function was determined in male Sprague-Dawley rats 6 weeks after surgical PAB. Through a left thoracotomy in rats weighing 180 to 200 g, a silk suture was tied tightly around an 18-gauge needle alongside the pulmonary artery. After subsequent rapid removal of the needle, a fixed constricted opening was created in the lumen equal to the diameter of the needle. Whereas the initial constriction was relatively mild, the combination of a fixed banding around the pulmonary artery and animal growth resulted in a progressive increase in RV systolic pressure and a pressure gradient of  $\approx$ 50 mm Hg after 6 weeks (see the online-only Data Supplement). In another subset of animals, an even greater degree of RV pressure overload was created by exposure to hypoxia (simulated altitude, 5000 m in a nitrogen dilution chamber) after the surgical procedure. Our objective was to mimic chronic progressive RV pressure overload, such as that which develops in human PAH, and not to induce acute severe pressure overload. The latter situation can be created by a much tighter constriction of the main pulmonary artery; this method has been used by several other investigators to mimic acute RV failure such as that which occurs in massive pulmonary embolism.<sup>16–18</sup> The PAB model was compared with a model featuring progressive pressure overload in conjunction with angioproliferative pulmonary vascular remodeling induced by the combined exposure to the VEGF receptor (VEGFR) blocker SU5416 and hypoxia (SuHx). This SuHx model is characterized by pulmonary vascular lesions that resemble those found in human PAH. The model was described in detail by our group previously.<sup>9,19</sup> Briefly, male Sprague-Dawley rats weighing 200 g received a single injection of SU5416 (20 mg/kg SC) and were exposed to a simulated altitude of 5000 m in a nitrogen dilution chamber for 4 weeks; thereafter,

the animals were kept at the altitude of Richmond, Va (sea level), for another 2 weeks. Before tissue harvests, echocardiographic measurements were made of the RV inner diameter and tricuspid annular plane systolic excursion. RV pressure-volume loops were assessed with a Millar catheter, and cardiac output was determined with thermodilution. Three-dimensional imaging of the RV microcirculation was achieved with intravital injections of fluorescent conjugated tomato lectin and subsequent confocal microscopy of whole-mount tissue sections. Immunohistochemistry and gene and protein expression studies were performed with standard procedures.

An alcohol-based extract of the dietary supplement Protandim (LifeVantage Corp, Littleton, Colo) was administered intraperitoneally every other day to an additional group of SuHx rats starting on the day before SU5416 injection. Protandim consists of 5 standardized ingredients (*Bacopa monniera*, *Silybum marianum*, *Withania somnifera*, green tea, and turmeric); although none of these components alone can induce a major increase in antioxidant enzymes, together they synergistically increase superoxide dismutase and heme-oxygenase-1 (HO-1).

See the online-only Data Supplement for additional Methods.

## Results

### Isolated RV Pressure Overload Is Not Associated With Heart Failure

Six weeks after surgery or SU5416 injection, the increase in RV systolic pressure was comparable in PAB and SuHx (the Table and Figure 1A). Consistent with previous studies,<sup>8,20</sup> RV function (determined by cardiac ultrasound and hemodynamic measurements) was preserved in PAB (Figure 1C and 1D). In contrast, SuHx rats showed overt signs of RV failure on cardiac ultrasound, with evidence of pericardial fluid, systolic paradox movement of the interventricular septum, RV dilatation (Figure 1C), and a reduced tricuspid annular plane systolic excursion (see the Table). Cardiac output was significantly decreased in SuHx but not in PAB (Figure 1D). The decreased RV function in SuHx rats was accompanied by exaggerated RV hypertrophy, with an increase in RV weight out of proportion to the degree of RV pressure overload (Figure 1B) and an increased rate of RV apoptosis (Figure 1E). Fetal gene reexpression, which has been demonstrated in endomyocardial biopsies of patients with PAH<sup>12</sup> and may be associated with a loss of myocardial contractility,<sup>21</sup> occurred both in the hypertrophied RV after PAB and in the failing RV of the SuHx model (online-only Data Supplement). Whereas mortality rates increase steeply after 6 weeks in the SuHx model, PAB was not associated with an increased long-term mortality. Cardiac ultrasound and cardiac output were still normal 22 weeks after PAB (Figure 1F).

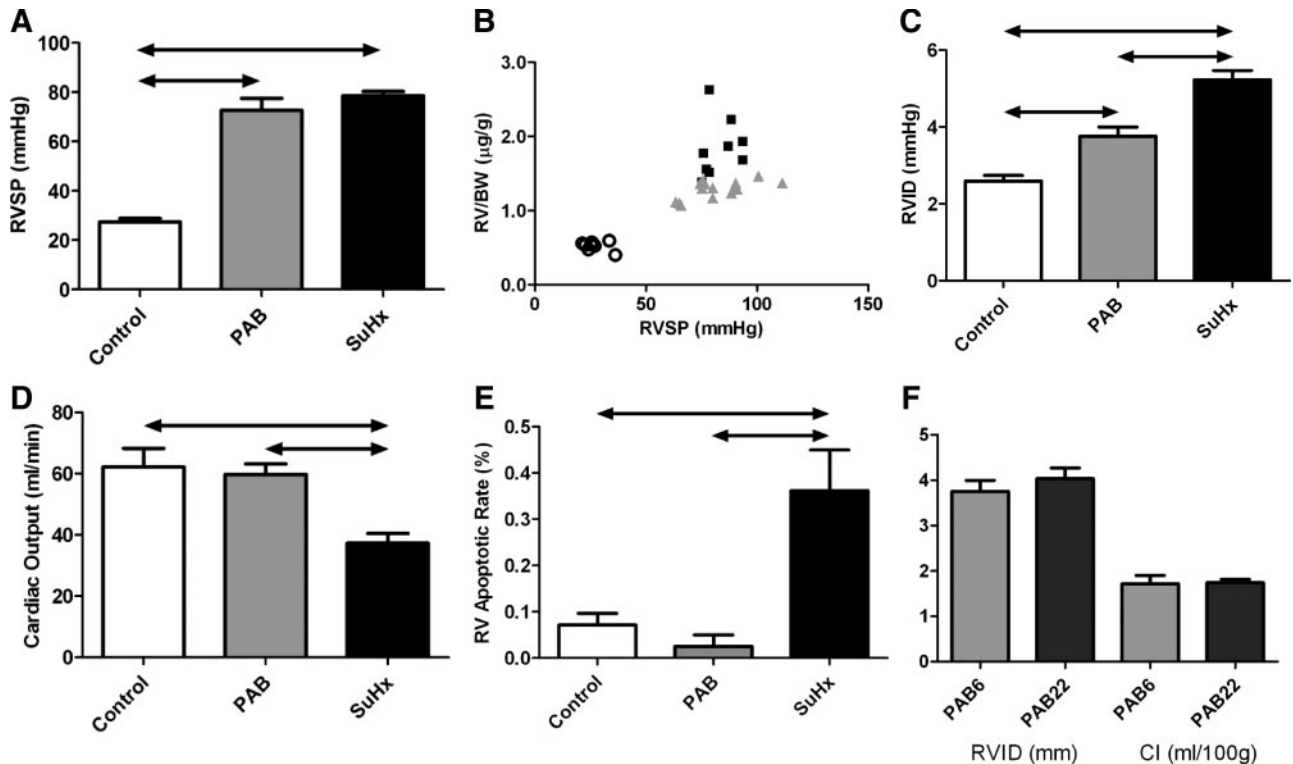


**Figure 1.** SuHx and isolated pressure overload by PAB generate the same increase in RV systolic pressure (RVSP) vs control rats (A; arrows denote significant differences between groups in posthoc testing), but SuHx is associated with more hypertrophy (calculated as micrograms RV weight per gram body weight [BW]) for a given degree of pressure overload (B; ○ indicates controls; ▲, PAB; and ■, SuHx) and more RV dilatation on cardiac ultrasound (C) than PAB. SuHx but not PAB is associated with a decreased cardiac output (D) and increased apoptosis rate (E), indicative of RV failure. RV function is maintained even 22 weeks after banding (PAB22), with only a minor increase in RV inner diameter in diastole and an unchanged cardiac output indexed for body weight (CI) vs 6 weeks after banding (PAB6).

### Angioproliferative PAH in the SuHx Model Is Associated With More RV Fibrosis and Oxidative Damage and Diminished Antioxidant Protection Compared With Isolated RV Pressure Overload

Cardiac fibrosis<sup>22,23</sup> and capillary rarefaction<sup>15</sup> can contribute to the development of LV failure in response to pressure overload. Whether these mechanisms contribute to PAH-associated RV failure is not clear. The degree of fibrosis assessed in trichrome-stained RV tissue sections was significantly greater in SuHx rats than in controls (Figure 2A, 2C, and 2G). The histological findings were confirmed by Western blots of collagen I (online-only Data Supplement). The development of fibrosis in SuHx animals was patchy, with no clear preference for specific RV segments or transmural regions. PAB was associated with an insignificant increase in RV fibrosis (Figure 2B and 2G). Associated with RV fibrosis and hypertrophy, gene expression of osteopontin-1 was increased in both models, but more so in SuHx than in PAB (Figure 3A).

Tissue fibrosis develops as a reparative response to oxidative damage,<sup>24</sup> and insufficient protection against an oxidant burden could explain the different degrees of fibrosis in our models. Figure 2D through 2F and 2H shows evidence of increased oxidative stress in SuHx compared with PAB; immunostaining with an antibody directed against malondialdehyde was more intense in the SuHx than PAB RV. We assessed protection from oxidant burden by examining the

expression of the antioxidant transcription factor nuclear factor E2-related factor 2 (Nrf2) and its target gene HO-1. Expression of both nuclear Nrf2 and HO-1 was significantly decreased in the RV of SuHx animals, thereby suggesting insufficient protection against oxidative stress (Figure 3E through 3G).

### Angioproliferative PAH in SuHx Is Associated With RV Capillary Rarefaction and Decreased VEGF microRNA and Protein Expression

RV capillary volume was significantly decreased in SuHx but not in PAB (Figure 4A through 4C and 4G). LV capillary volume was normal in both models. RV capillaries appeared morphologically heterogeneous in SuHx; this finding was best appreciated in 3-dimensional reconstructions (see the video in the online-only Data Supplement). In some areas, capillaries appeared narrow and pruned; others were dilated and irregularly shaped. Staining with an anti-CD31 antibody confirmed a decreased capillary density in the SuHx RV compared with control and PAB (Figure 4D through 4F and 4H). These results indicate that some components of the lung vascular changes in the SuHx model, and not pressure-overload per se, are linked to changes in the RV microcirculation.

VEGF is a critical determinant of capillary growth and maintenance. Whereas the expression of VEGF, VEGFR1, and VEGFR2 messenger RNA (mRNA) was decreased in the

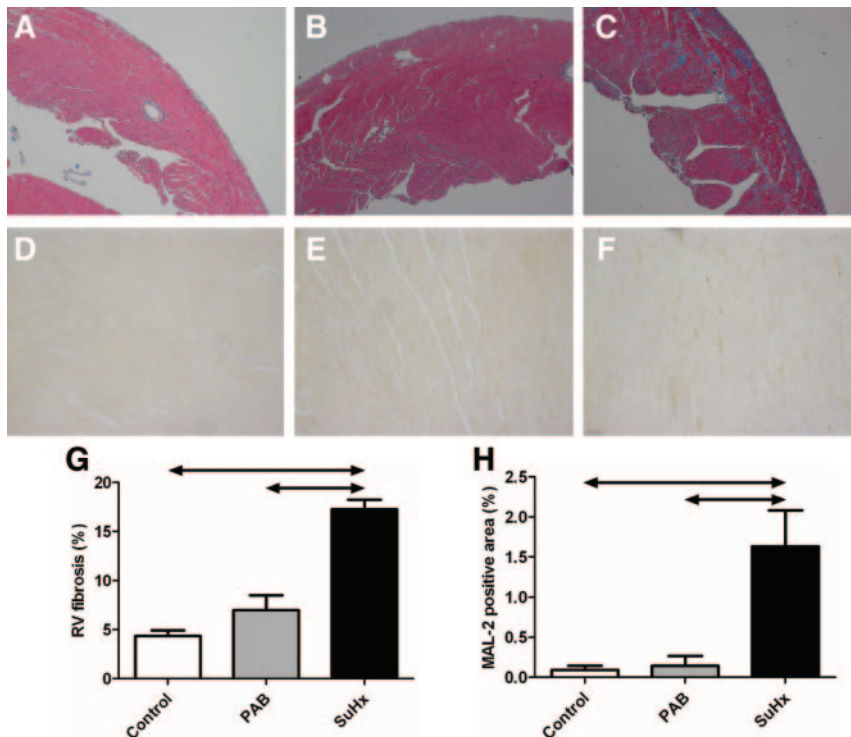


**Figure 2.** Masson trichrome stain showing extensive RV fibrosis in SuHx (C) but not in PAB (B) or controls (A). Fibrotic areas are distributed randomly across the RV free walls. G, Fibrosis quantification (blue-stained areas expressed as percentage of total RV surface area) of digitized images. Staining with malondialdehyde antibodies shows evidence of oxidative stress in the SuHx RV but not PAB RV (D through F and H).

RV of SuHx animals (Figure 3B through 3D), expression was significantly increased in the corresponding LV (online-only Data Supplement). No significant changes were observed in the RV or LV of PAB animals (in fact, there was a trend toward increased VEGF mRNA in the PAB RV). Western blots showed decreased VEGF protein expression in the RVs in both models but a more pronounced decrease in SuHx (Figure 5D). Because HIF-1 $\alpha$  is a major controller of VEGF expression, we examined nuclear HIF-1 $\alpha$  expression in these same RVs. As shown in Figure 5D and 5E, there is an apparent uncoupling of VEGF transcription from stable HIF-1 $\alpha$  protein expression; the strongest signal for HIF-1 $\alpha$  protein is observed in the SuHx RV, which is characterized by decreased VEGF expression. To further assess the importance of capillary rarefaction in the transition from adaptive hypertrophy to RV failure, we fed an additional group of PAB rats a low-copper diet, an intervention known to interfere with HIF-1 $\alpha$  protein stabilization and angiogenesis in the LV adapting to pressure overload.<sup>25</sup> As expected, this intervention resulted in RV fibrosis, capillary rarefaction, and failure (online-only Data Supplement).

### The RV Adaptive Response to Pressure Overload Is Not Directly Affected by SU5416 or Exposure to Hypoxia

Only the SuHx combination leads to severe angioproliferative pulmonary hypertension; either intervention alone (SU5416 or hypoxia) is insufficient to induce PAH and/or RV failure.<sup>9</sup> No fibrosis was seen in the LVs of rats in any of the single-intervention models, and LV capillary volume and morphology were similar in the single-intervention conditions (and equal to the capillary volume of the normal RV; not shown). This strongly suggests that fibrosis, capillary alter-

tations, and RV dysfunction in the SuHx model are not a direct consequence of either SU5416 or hypoxia alone. To further exclude the possibility that SU5416 or hypoxic exposure specifically interferes with RV adaptation to pressure overload, a separate group of rats were subjected to PAB in combination with either SU5416 administration or hypoxic exposure. Neither combination was associated with signs of RV failure by cardiac ultrasound (Figure 5A), nor was the degree of RV hypertrophy induced by PAB affected by SU5416 or hypoxia (Figure 5C). However, and remarkably, RV systolic pressure after PAB was even higher when combined with hypoxic exposure (range, 90 to 125 mm Hg; average,  $109 \pm 14$  mm Hg; Figure 5B), documenting a considerable pressure resiliency of the RV. Exposure to either SU5416 or hypoxia of PAB rats did not change the capillary volume or protein expressions of HIF-1 $\alpha$ , VEGF, Nrf2, or HO-1 (Figure 5D through 5F).

### Induction of Nrf2 and HO-1 in SuHx Rats by Dietary Intervention Is Associated With Diminished Oxidative Stress, Prevention of Maladaptive RV Remodeling, and Improved RV Function Despite Persisting Pulmonary Vascular Changes

We hypothesized that attenuating the oxidative stress in the SuHx model would improve VEGF expression, reduce RV fibrosis, restore RV capillarization, and improve RV function. To this end, we treated a separate group of SuHx rats with Protandim, a plant extract that induces Nrf2-dependent, antioxidant cardioprotective enzymes.<sup>26</sup> Whereas Protandim treatment of SuHx rats did not decrease the number of occluded pulmonary vascular lesions and did not result in a decreased pulmonary artery pressure (Figure 6A through 6C),

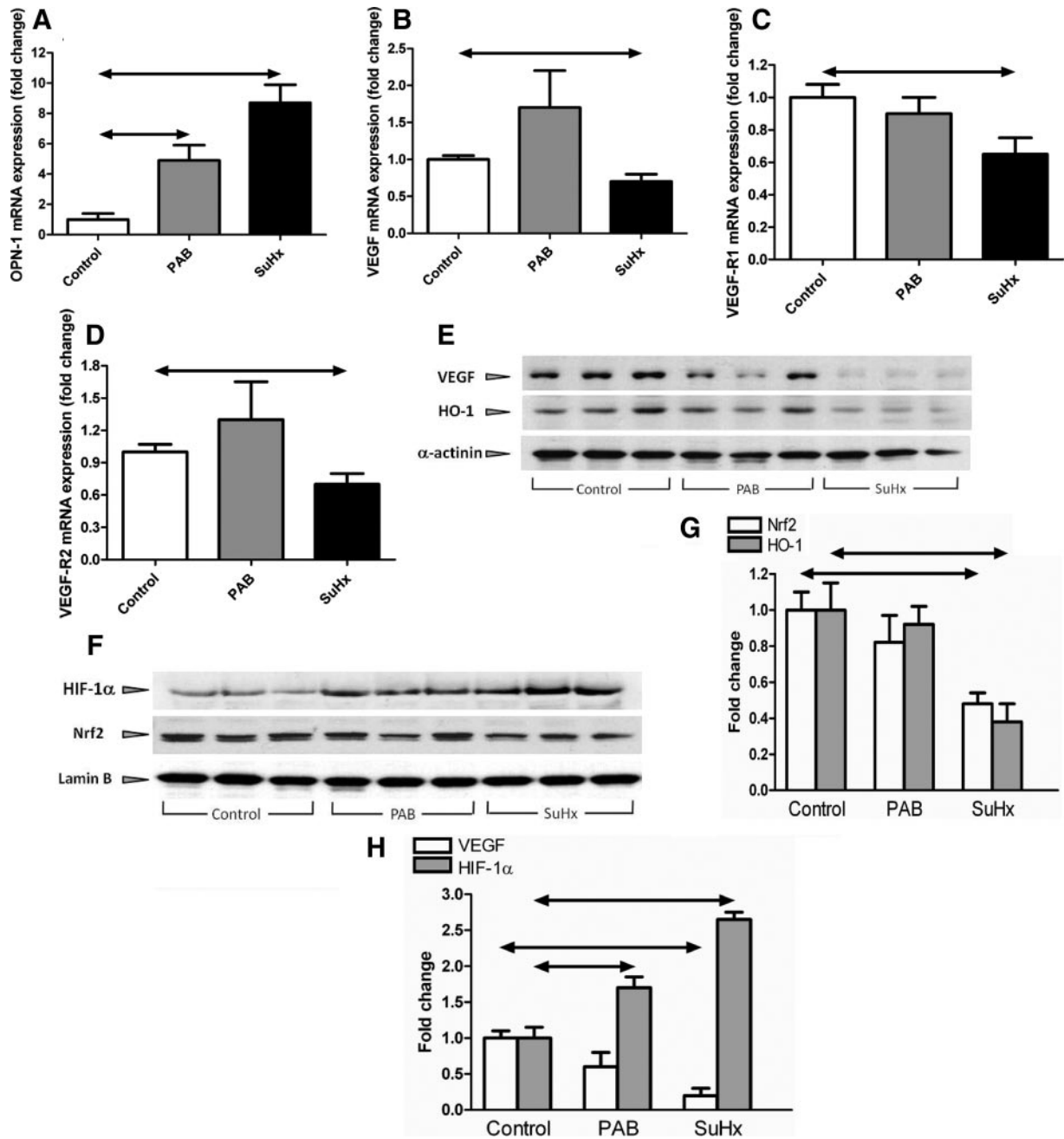


**Figure 3.** After PAB and even more after SuHx, an increased gene expression of osteopontin-1 (OPN-1; A) is found. Gene expression of VEGF (B), VEGFR1 (C), and VEGFR2 (D) is decreased in the RV of SuHx-exposed animals but not in the RV after PAB. VEGF protein levels are also decreased after SuHx but not after PAB (E and H). In F and H, there is an apparent uncoupling of VEGF transcription from stable nuclear HIF-1 $\alpha$  protein expression; the strongest signal for HIF-1 $\alpha$  protein is observed in the RV from SuHx-treated animals. The increased degree of RV oxidative stress may be related to a decreased antioxidant protection resulting from suppression of Nrf2-dependent expression of HO-1 in SuHx (D through G).

our data point to a cardioprotective effect of Protandim: (1) The expression of Nrf2 and HO-1 was upregulated after Protandim (Figure 6H and 6I); (2) the suppression of microRNA (miRNA)-208 expression was attenuated (miRNA-208 increased to levels seen in PAB; see the online-only Data Supplement) while osteopontin-1 expression was diminished by Protandim (Figure 6G); (3) nuclear HIF-1 $\alpha$  protein expression was decreased after Protandim treatment while VEGF mRNA expression was preserved and VEGF protein expression in the RV was increased

(Figure 6I); and (4) RV fibrosis was attenuated and RV capillary density was preserved after Protandim treatment (Figure 6E and 6F), all of which were accompanied by a preserved cardiac output (Figure 6D), less dilatation on cardiac ultrasound, and a decreased rate of RV myocardial apoptosis (online-only Data Supplement).

### Discussion

In this study, we show that chronic progressive RV pressure overload per se does not lead to severe RV dysfunction and

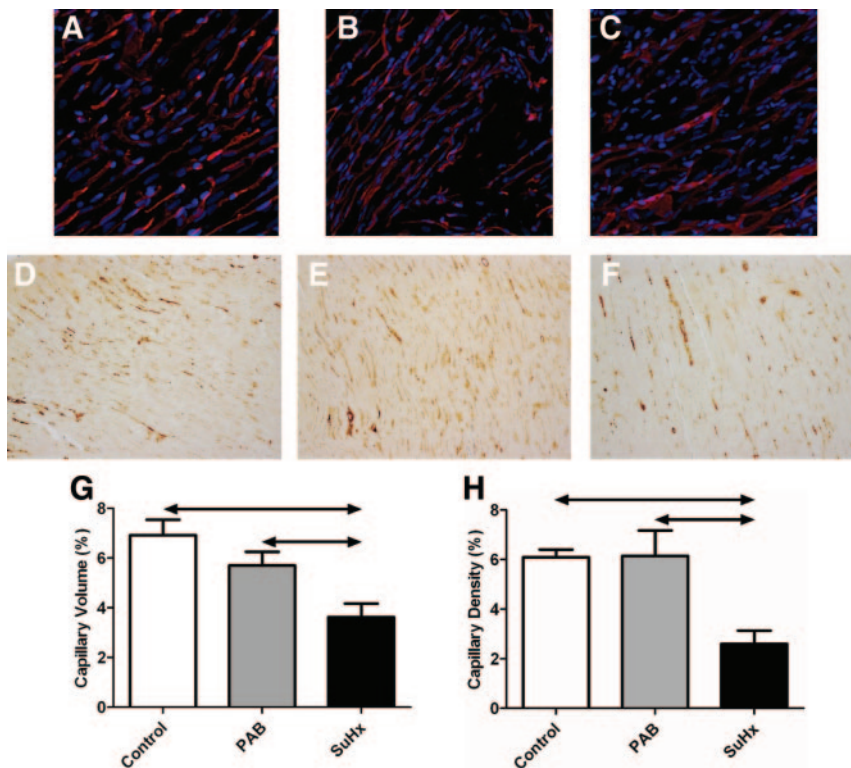


**Figure 4.** Confocal images of lectin-stained RV microvessels (in vivo perfusion with tomato lectin stains red; DAPI staining of nuclei is blue). Capillaries in the SuHx model (C) are less abundant and are morphologically heterogeneous (best appreciated in the online-only Data Supplement Movie), whereas capillaries in PAB (B) resemble those in controls (A). Capillary volume (expressed as percentage of tissue volume) is significantly decreased in SuHx vs controls and PAB (G). E, F, and H. A similar decrease in capillary density as assessed by anti-CD31 staining.

that RV failure in experimental PAH is associated with myocardial fibrosis and capillary rarefaction. We also demonstrate that RV failure is associated with decreased RV VEGF protein expression and impaired myocardial VEGF transcription despite increased HIF-1 $\alpha$  protein levels. We further show that induction of Nrf2 by the herbal supplement Protandim prevents cardiac oxidative stress, preserves HO-1 and VEGF expression and myocardial capillary density, and prevents RV failure without modifying lung angioproliferation.

The development of RV failure in the SuHx model cannot be attributed to VEGFR blockade interfering with RV adaptation to pressure overload. SU5416 treatment without hypoxia (ie, without the induction of angioproliferative lesions) is not associated with failure of the pressure overloaded RV or with a decreased myocardial capillary density. Combined exposure to SU5416 and hypoxia does not lead to changes in VEGF signaling or a reduced capillary density in the LV. SU5416 injection in PAB rats does not interfere with RV adaptation to pressure overload.

It is frequently assumed that the elevated pulmonary artery pressure (RV afterload) is the main and perhaps only cause of PAH-associated RV failure. However, our data provide evidence that the increased afterload alone does not cause the rat RV to fail; in fact, after PAB, the RV hypertrophies and maintains a high systolic pressure and a normal cardiac output. After PAB, the degree of hypertrophy follows a close linear relationship with the RV systolic pressure, whereas the degree of hypertrophy for a given pressure is exaggerated in SuHx. In PAB rats, the RV chamber is not dilated, the degree of myocardial fibrosis is limited, and the capillary density remains normal. The RV after PAB demonstrates a decreased miRNA-208 expression, consistent with an  $\alpha/\beta$ -myosin

heavy chain switch,<sup>27</sup> but this phenomenon is apparently not a marker of RV failure. A decreased  $\alpha$ -myosin heavy chain expression has also been observed in chronic hypoxic pulmonary hypertension, as stated, without signs of RV failure.<sup>28</sup> Maintained RV performance up to 12 weeks after PAB has also been reported by Faber et al.<sup>8,29</sup> In the present study, we extended this observation to 22 weeks after PAB without evidence of RV failure. Additionally, the experiment in which PAB was combined with hypoxic exposure shows that the RV systolic pressure can increase to a level that is equal to the normal LV systolic pressure (far above the pressure seen in conventional models of pulmonary hypertension) without signs of RV failure. This set of experiments demonstrates that even a combination of a central obstruction and peripheral vascular changes (hypoxic vasoconstriction and vascular remodeling without angioproliferation) is insufficient to make the RV fail.

RV fibrotic changes in the 2 models paralleled changes in the cardiac expression of the phosphoprotein osteopontin-1 (discussed further in the online-only Data Supplement). Although at present data that link RV fibrosis to oxidative stress are lacking, on the basis of findings in models of liver and lung fibrosis, we postulate that different degrees of oxidative damage could have accounted for the different degrees of fibrosis in SuHx and PAB. As shown previously, antioxidant enzymes (eg, thioredoxin and catalase) are up-regulated after PAB.<sup>29</sup> Catalase expression is under the influence of the transcription factor Nrf2.<sup>30</sup> Nrf2 regulates inducible expression of antioxidant response element-containing genes,<sup>31</sup> encoding proteins that play important roles in the adaptive responses to oxidative stress [apart from catalase, eg, HO-1, NAD(P)H:quinone oxidoreductase, glutathi-

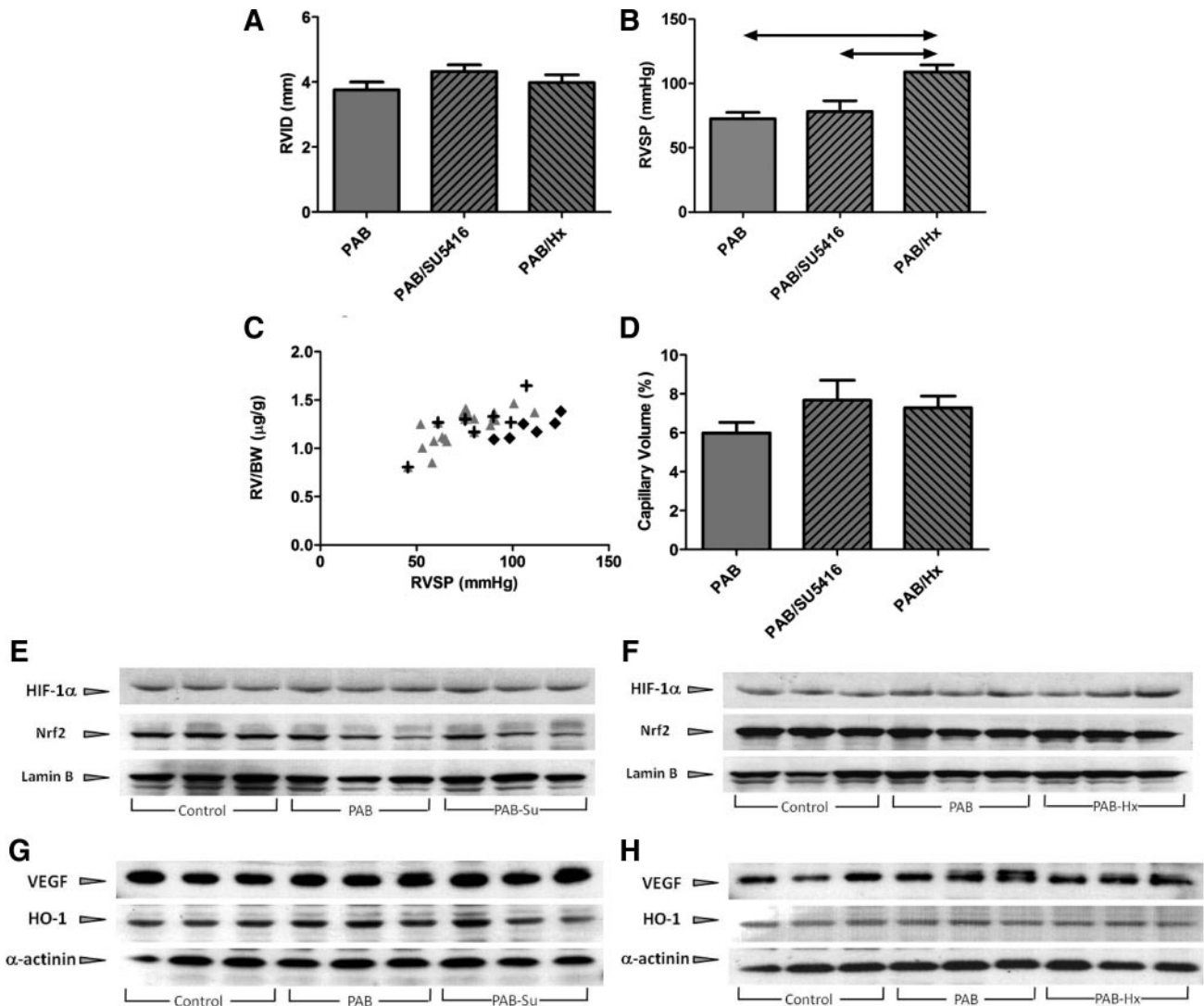


**Figure 5.** To exclude the possibility that VEGFR blockade specifically interferes with the capacity of the RV to adapt to pressure overload, rats were injected with 20 mg/kg SU5416 on day 3 after surgical PAB. Similarly, to exclude the possibility that hypoxia induces a transition from compensated hypertrophy to RV failure after PAB, banded rats were exposed to hypoxia for 4 weeks, starting 3 days after surgery. Neither of these interventions was associated with signs of RV failure on cardiac ultrasound (A) 6 weeks after surgery. Exposure of PAB rats to SU5416 or hypoxia resulted in a degree of RV hypertrophy that was similar to that in the PAB-only experiments (C;  $\Delta$  indicates PAB;  $\blacklozenge$ , PAB plus hypoxia; and  $+$ , PAB plus SU5416). RV systolic pressure (RVSP) after PAB was even higher when combined with hypoxia (B; individual RVSPs ranging from 90 to 125 mm Hg), pointing to a considerable pressure resiliency of the RV. There was no difference in capillary density or protein expression of HIF-1 $\alpha$ , VEGF, Nrf2, and HO-1 between the 3 conditions (D through F).

one S-transferase, and  $\gamma$ -glutamylcysteine synthase].<sup>32–36</sup> A recent study by Yet et al<sup>37</sup> demonstrated RV failure in HO-1 knockout mice exposed to chronic hypoxia, suggesting that HO-1 plays an important role in maintaining RV function; interestingly, the dilated RV tissue in the study by Yet et al showed signs of oxidative stress and fibrosis. Our experiments show that the increased degree of fibrosis in the SuHx model is paralleled by a decreased expression of Nrf2 and HO-1.

Angioproliferative PAH in the SuHx model was paradoxically associated with a loss of RV capillaries, whereas isolated RV pressure overload in the PAB model was not. RV capillary loss after PAB could be induced by dietary copper restriction, which also induced RV failure (online-only Data Supplement). Capillary rarefaction has not been systematically studied as a cause of RV failure, despite the fact that a reduced capillary density and VEGF protein expression are

known to play causative roles in pressure overload–induced LV failure.<sup>11,15,38</sup> Chronic RV overload in monocrotaline-induced pulmonary hypertension is associated with a reduced capillary density and reduced VEGF expression, whereas RV capillary density and VEGF expression are increased in chronic hypoxic pulmonary hypertension.<sup>14</sup> Here, we show that preservation of the RV microcirculation is associated with maintained RV function. In the murine LV, transverse aortic constriction leads initially to upregulation of LV VEGF signaling, but after 2 weeks, VEGF signaling becomes insufficient and is associated with decreased cardiac microvascular density and systolic dysfunction. Restoration of VEGF signaling leads to a normalization of capillary density and an improvement in systolic function.<sup>15</sup> These changes may be related to a time-dependent effect of Akt1 activation on VEGF expression; short-term activation of Akt1 leads to

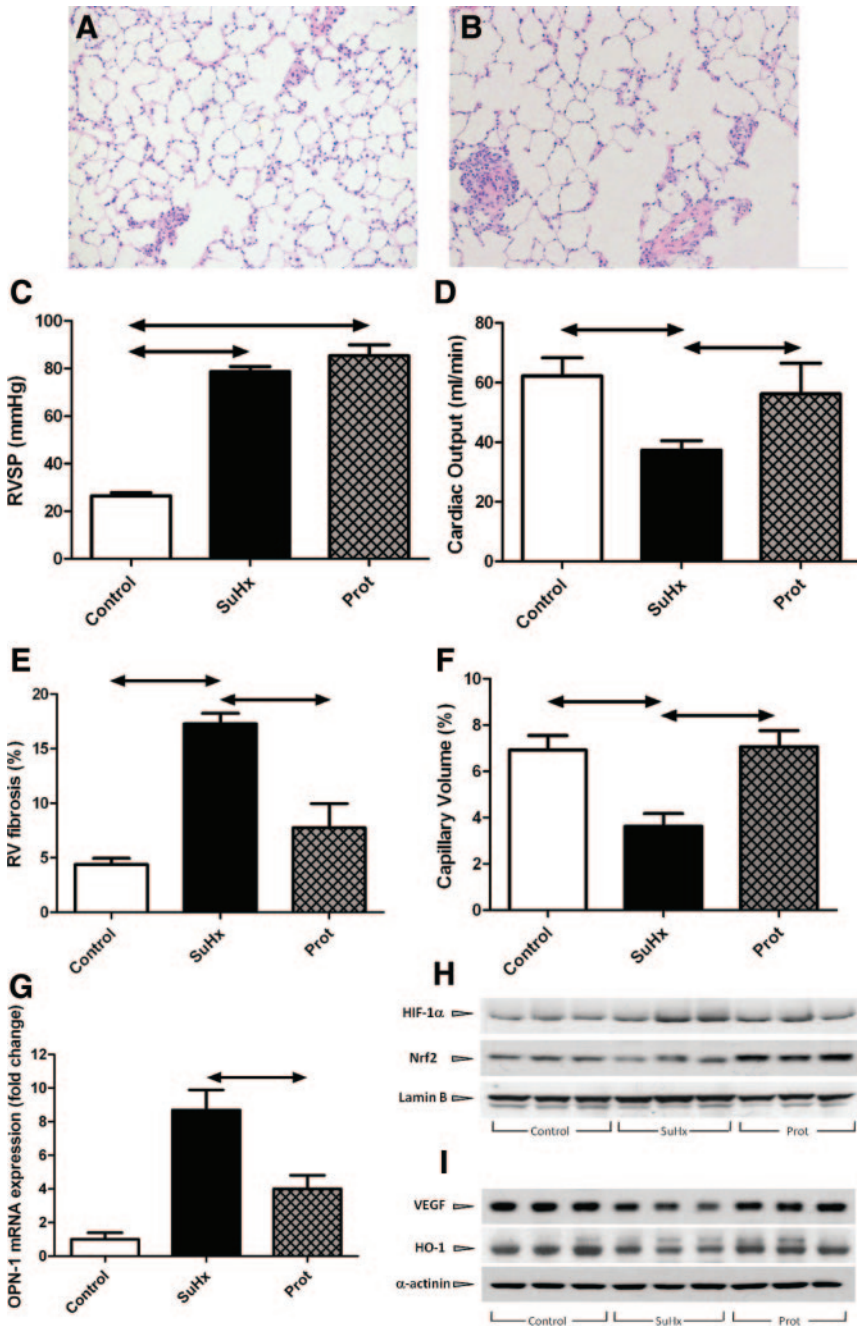


**Figure 6.** Protandim (Prot) treatment in SuHx has no effect on pulmonary vascular remodeling (controls in A, Protandim-treated animals in B) or RV systolic pressure (RVSP; C) but improves cardiac function (increased cardiac output in D) and prevents maladaptive RV remodeling (decreased RV fibrosis in E; maintained capillary density in F). Protandim treatment is associated with decreased RV mRNA expression of osteopontin-1 (G), upregulation of Nrf2 and HO-1 (H and I), decreased stabilization of nuclear HIF-1 $\alpha$  (H), and preserved VEGF protein expression (I). For densitometry of the Western blots, see the online-only Data Supplement.

adaptive cardiac hypertrophy together with increased cardiomyocyte VEGF secretion and angiogenesis, whereas long-term Akt1 activation is associated with cardiac dilatation, decreased VEGF secretion, and capillary rarefaction.<sup>11</sup>

In our study, the decrease in VEGF expression may have been caused by an apparent uncoupling of HIF-1 $\alpha$  and VEGF transcription; the lowest levels of RV VEGF mRNA were found in SuHx despite the highest expression of nuclear HIF-1 $\alpha$  (Figure 4). This finding differs from data obtained in the pressure-overloaded murine LV, where p53-induced suppression of HIF-1 $\alpha$  leads to decreased VEGF expression.<sup>15</sup> We propose that abundant oxidative stress (along with impaired antioxidant defenses) in the SuHx model may have led to a decreased VEGF protein expression via damage to the

hypoxia response element of the VEGF promoter, making the VEGF gene less sensitive to regulation by HIF-1 $\alpha$ .<sup>39</sup> Induction of Nrf2 and HO-1 expression by Protandim was associated with a reduction in oxidative stress and fibrosis, preservation of the RV microcirculation, and maintained RV function. Along with the reduction in RV fibrosis, mRNA expression of osteopontin-1 was reduced. The reduction in nuclear HIF-1 $\alpha$  protein expression with Protandim may be a marker of reduced myocardial hypoxia, and we speculate that induction of HO-1 may have resulted in preserved VEGF protein expression by preventing oxidative damage to the VEGF promoter.<sup>39</sup>

### Conclusions

Chronic progressive pressure overload in the context of angioproliferative pulmonary hypertension, but not in isola-

tion, is associated with RV fibrosis, capillary rarefaction, and RV failure. RV failure is associated with oxidative stress and reduced HO-1–dependent antioxidant protection. Restoration of Nrf2 and HO-1 signaling can prevent maladaptive RV remodeling and preserve RV function. This study does not address the reason why angioproliferative pulmonary hypertension is associated with a failing antioxidant defense. We can only speculate that the structurally altered pulmonary circulation in PAH releases mediators that interfere with adaptive RV responses already maximally challenged to meet the increased mechanical stress. Candidate factors and mediators are immune cells activated within the pulmonary vascular wall, subsequently infiltrating the heart and releasing chemokines and/or antibodies;<sup>40</sup> hormones that the pulmonary vasculature produces or fails to metabolize, eg, angiotensin II<sup>41</sup> and endothelin-1<sup>42</sup>; and neuronal reflex mechanisms with afferents stimulated in the “sick lung circulation” and efferents affecting RV function.

### Sources of Funding

This work was supported by funds from the Victoria Johnson Center for Obstructive Lung Disease Research. Dr Bogaard received a Dekker stipend from the Netherlands Heart Foundation, grant 2006T022. Microscopy was performed at the Virginia Commonwealth University, Department of Neurobiology and Anatomy Microscopy Facility, supported in part by funding from National Institutes of Health–National Institute of Neurological Disorders and Stroke Center core grant (5P30NS047463).

### Disclosures

Dr McCord served as consultant for LifeVantage Corp, Littleton, Colo. The other authors report no conflicts.

### References

- Simonneau G, Galie N, Rubin LJ, Langleben D, Seeger W, Domenighetti G, Gibbs S, Lebrech D, Speich R, Beghetti M, Rich S, Fishman A. Clinical classification of pulmonary hypertension. *J Am Coll Cardiol*. 2004; 43(suppl S):S5–S12S.
- D'Alonzo GE, Barst RJ, Ayres SM, Bergofsky EH, Brundage BH, Detre KM, Fishman AP, Goldring RM, Groves BM, Kernis JT. Survival in patients with primary pulmonary hypertension: results from a national prospective registry. *Ann Intern Med*. 1994;115:343–349.
- Zornoff LA, Skali H, Pfeffer MA, St John SM, Rouleau JL, Lamas GA, Plappert T, Rouleau JR, Moye LA, Lewis SJ, Braunwald E, Solomon SD. Right ventricular dysfunction and risk of heart failure and mortality after myocardial infarction. *J Am Coll Cardiol*. 2002;39:1450–1455.
- Ghio S, Gavazzi A, Campana C, Inzerra C, Klersy C, Sebastiani R, Arbustini E, Recusani F, Tavazzi L. Independent and additive prognostic value of right ventricular systolic function and pulmonary artery pressure in patients with chronic heart failure. *J Am Coll Cardiol*. 2001;37: 183–188.
- Weitzenblum E, Hirth C, Ducolone A, Mirhom R, Rasaholjanahary J, Ehrhart M. Prognostic value of pulmonary artery pressure in chronic obstructive pulmonary disease. *Thorax*. 1981;36:752–758.
- Bogaard HJ, Abe K, Vonk-Noordegraaf A, Voelkel NF. The right ventricle under pressure; cellular and molecular mechanisms of right heart failure in pulmonary hypertension. *Chest*. 2009;135:794–804.
- Gudausky TM, Beekman RH III. Current options, and long-term results for interventional treatment of pulmonary valvar stenosis. *Cardiol Young*. 2006;16:418–427.
- Faber MJ, Dalinghaus M, Lankhuizen IM, Steendijk P, Hop WC, Schoemaker RG, Duncker DJ, Lamers JMJ, Helbing WA. Right and left ventricular function after chronic pulmonary artery banding in rats assessed with biventricular pressure-volume loops. *Am J Physiol Heart Circ Physiol*. 2006;291:H1580–H1586.
- Taraseviciene-Stewart L, Kasahara Y, Alger L, Hirth P, McMahon G, Waltenberger J, Voelkel NF, Tudor RM. Inhibition of the VEGF receptor 2 combined with chronic hypoxia causes cell death-dependent pulmonary endothelial cell proliferation and severe pulmonary hypertension. *FASEB J*. 2001;15:427–438.
- Gradman AH, Alfayoumi F. From left ventricular hypertrophy to congestive heart failure: management of hypertensive heart disease. *Prog Cardiovasc Dis*. 2006;48:326–341.
- Shiojima I, Sato K, Izumiya Y, Schiekofer S, Ito M, Liao R, Colucci WS, Walsh K. Disruption of coordinated cardiac hypertrophy and angiogenesis contributes to the transition to heart failure. *J Clin Invest*. 2005; 115:2108–2118.
- Lowes BD, Minobe W, Abraham WT, Rizeq MN, Bohlmeier TJ, Quaipe RA, Roden RL, Dutcher DL, Robertson AD, Voelkel NF, Badesch DB, Groves BM, Gilbert EM, Bristow MR. Changes in gene expression in the intact human heart: downregulation of alpha-myosin heavy chain in hypertrophied, failing ventricular myocardium. *J Clin Invest*. 1997;100: 2315–2324.
- Gomez A, Bialostozky D, Zajarias A, Santos E, Palomar A, Martinez ML, Sandoval J. Right ventricular ischemia in patients with primary pulmonary hypertension. *J Am Coll Cardiol*. 2001;38:1137–1142.
- Partovian C, Adnot S, Eddahibi S, Teiger E, Levame M, Dreyfus P, Raffestin B, Frelin C. Heart and lung VEGF mRNA expression in rats with monocrotaline- or hypoxia-induced pulmonary hypertension. *Am J Physiol*. 1998;275(pt 2):H1948–H1956.
- Sano M, Minamino T, Toko H, Miyauchi H, Orimo M, Qin Y, Akazawa H, Tateno K, Kayama Y, Harada M, Shimizu I, Asahara T, Hamada H, Tomita S, Molkentin JD, Zou Y, Komuro I. p53-Induced inhibition of Hif-1 causes cardiac dysfunction during pressure overload. *Nature*. 2007; 446:444–448.
- Vlahakes GJ, Turley K, Hoffman JI. The pathophysiology of failure in acute right ventricular hypertension: hemodynamic and biochemical correlations. *Circulation*. 1981;63:87–95.
- Kerbaul F, Rondelet B, Demester JP, Fesler P, Huez S, Naeije R, Brimiouille S. Effects of levosimendan versus dobutamine on pressure load-induced right ventricular failure. *Crit Care Med*. 2006;34:2814–2819.
- Welham KC, Silove ED, Wyse RK. Experimental right ventricular hypertrophy and failure in swine. *Cardiovasc Res*. 1978;12:61–65.
- Oka M, Homma N, Taraseviciene-Stewart L, Morris KG, Kraskauskas D, Burns N, Voelkel NF, McMurry IF. Rho kinase-mediated vasoconstriction is important in severe occlusive pulmonary arterial hypertension in rats. *Circ Res*. 2007;100:923–929.
- Faber MJ, Dalinghaus M, Lankhuizen IM, Bezstarosti K, Verhoeven AJ, Duncker DJ, Helbing WA, Lamers JM. Time dependent changes in cytoplasmic proteins of the right ventricle during prolonged pressure overload. *J Mol Cell Cardiol*. 2007;43:197–209.
- Herron TJ, McDonald KS. Small amounts of alpha-myosin heavy chain isoform expression significantly increase power output of rat cardiac myocyte fragments. *Circ Res*. 2002;90:1150–1152.
- Khan R, Sheppard R. Fibrosis in heart disease: understanding the role of transforming growth factor-beta in cardiomyopathy, valvular disease and arrhythmia. *Immunology*. 2006;118:10–24.
- Weber KT, Janicki JS, Shroff SG, Pick R, Chen RM, Bashey RI. Collagen remodeling of the pressure-overloaded, hypertrophied nonhuman primate myocardium. *Circ Res*. 1988;62:757–765.
- Kisseleva T, Brenner DA. Mechanisms of fibrogenesis. *Exp Biol Med (Maywood)*. 2008;233:109–122.
- Jiang Y, Reynolds C, Xiao C, Feng W, Zhou Z, Rodriguez W, Tyagi SC, Eaton JW, Saari JT, Kang YJ. Dietary copper supplementation reverses hypertrophic cardiomyopathy induced by chronic pressure overload in mice. *J Exp Med*. 2007;204:657–666.
- Nelson SK, Bose SK, Grunwald GK, Myhill P, McCord JM. The induction of human superoxide dismutase and catalase in vivo: a fundamentally new approach to antioxidant therapy. *Free Radic Biol Med*. 2006;40:341–347.
- Van Rooij E, Sutherland LB, Qi X, Richardson JA, Hill J, Olson EN. Control of stress-dependent cardiac growth and gene expression by a microRNA. *Science*. 2007;316:575–579.
- Nakanishi K, Nakata Y, Kanazawa F, Imamura S, Matsuoka R, Osada H, Kawai T, Uenoyama M, Aures T, Ikeda T. Changes in myosin heavy chain and its localization in rat heart in association with hypobaric hypoxia-induced pulmonary hypertension. *J Pathol*. 2002;197:380–387.
- Faber MJ, Dalinghaus M, Lankhuizen IM, Bezstarosti K, Verhoeven AJ, Duncker DJ, Helbing WA, Lamers JM. Time dependent changes in cytoplasmic proteins of the right ventricle during prolonged pressure overload. *J Mol Cell Cardiol*. 2007;43:197–209.
- Zhu H, Jia Z, Zhang L, Yamamoto M, Misra HP, Trush MA, Li Y. Antioxidants and phase 2 enzymes in macrophages: regulation by Nrf2

- signaling and protection against oxidative and electrophilic stress. *Exp Biol Med (Maywood)*. 2008;233:463–474.
31. Chan K, Kan YW. Nrf2 is essential for protection against acute pulmonary injury in mice. *Proc Natl Acad Sci U S A*. 1999;96:12731–12736.
  32. Venugopal R, Jaiswal AK. Nrf2 and Nrf1 in association with Jun proteins regulate antioxidant response element-mediated expression and coordinated induction of genes encoding detoxifying enzymes. *Oncogene*. 1998;17:3145–3156.
  33. Alam J, Stewart D, Touchard C, Boinapally S, Choi AM, Cook JL. Nrf2, a Cap'n'Collar transcription factor, regulates induction of the heme oxygenase-1 gene. *J Biol Chem*. 1999;274:26071–26078.
  34. Wild AC, Moinova HR, Mulcahy RT. Regulation of gamma-glutamylcysteine synthetase subunit gene expression by the transcription factor Nrf2. *J Biol Chem*. 1999;274:33627–33636.
  35. Ishii T, Itoh K, Takahashi S, Sato H, Yanagawa T, Katoh Y, Bannai S, Yamamoto M. Transcription factor Nrf2 coordinately regulates a group of oxidative stress-inducible genes in macrophages. *J Biol Chem*. 2000;275:16023–16029.
  36. Huang HC, Nguyen T, Pickett CB. Regulation of the antioxidant response element by protein kinase C-mediated phosphorylation of NF-E2-related factor 2. *Proc Natl Acad Sci U S A*. 2000;97:12475–12480.
  37. Yet SF, Perrella MA, Layne MD, Hsieh CM, Maemura K, Kobzik L, Wiesel P, Christou H, Kourembanas S, Lee ME. Hypoxia induces severe right ventricular dilatation and infarction in heme oxygenase-1 null mice. *J Clin Invest*. 1999;103:R23–R29.
  38. Izumiya Y, Shiojima I, Sato K, Sawyer DB, Colucci WS, Walsh K. Vascular endothelial growth factor blockade promotes the transition from compensatory cardiac hypertrophy to failure in response to pressure overload. *Hypertension*. 2006;47:887–893.
  39. Grishko V, Solomon M, Breit JF, Killilea DW, Ledoux SP, Wilson GL, Gillespie MN. Hypoxia promotes oxidative base modifications in the pulmonary artery endothelial cell VEGF gene. *FASEB J*. 2001;15:1267–1269.
  40. Taraseviciene-Stewart L, Nicolls MR, Kraskauskas D, Scerbavicius R, Burns N, Cool C, Wood K, Parr JE, Boackle SA, Voelkel NF. Absence of T cells confers increased pulmonary arterial hypertension and vascular remodeling. *Am J Respir Crit Care Med*. 2007;175:1280–1289.
  41. Langleben D, Orfanos SE, Giovinazzo M, Hirsch A, Baron M, Senecal JL, Armaganidis A, Catravas JD. Pulmonary capillary endothelial metabolic dysfunction: severity in pulmonary arterial hypertension related to connective tissue disease versus idiopathic pulmonary arterial hypertension. *Arthritis Rheum*. 2008;58:1156–1164.
  42. Dupuis J, Stewart DJ, Cernacek P, Gosselin G. Human pulmonary circulation is an important site for both clearance and production of endothelin-1. *Circulation*. 1996;94:1578–1584.

### CLINICAL PERSPECTIVE

The presence of right heart failure increases the morbidity and mortality associated with pulmonary hypertension. The mechanisms by which right heart failure occurs in pulmonary hypertension are uncertain; however, the degree and duration of pressure overload do not explain sufficiently why the right ventricle (RV) ultimately dilates and fails. The present study shows in a rodent model that the RV is tolerant to chronic progressive pressure overload as long as this pressure overload is not associated with angioproliferative pulmonary vascular disease. This finding suggests that molecular, cellular, and hemodynamic lung-heart interactions explain the transition from compensated hypertrophy to RV dilatation and failure in pulmonary hypertension. It is further shown that important features of the failing RV include a loss of capillaries in the microcirculation and increased fibrosis. These structural changes are associated with evidence of oxidative stress and a biochemical uncoupling of hypoxia-induced factor-1 $\alpha$  protein stabilization and vascular endothelial growth factor transcription. Moreover, this study shows that a dietary intervention can prevent RV dysfunction and pathological remodeling in the setting of persistent pressure overload. By inducing nuclear factor E2-related factor 2 and heme-oxygenase 1, the herbal supplement Protandim prevented a loss of myocardial capillaries, reduced the degree of RV fibrosis, and prevented RV dilation and loss of myocardial contractility.

## **SUPPLEMENTAL MATERIAL**

### **Supplemental Methods**

Using a direct comparison in rats of similar age, strain and degree of pressure overload, RV function was evaluated by echocardiography, thermodilution and pressure-volume analysis. RV morphology was ascertained using immunohistochemistry and microcirculatory imaging. Relevant signaling pathways were interrogated by Western Blotting and qPCR.

#### *SuHx model*

This model requires the combined action of the VEGF receptor antagonist SU5416 and chronic hypoxia. Male Sprague-Dawley rats weighing 200g are injected subcutaneously (s.c.) with SU5416 suspended in 0.5% (w/v) carboxymethylcellulose sodium, 0.9% (w/v) sodium chloride, 0.4% (v/v) polysorbate 80, 0.9% (v/v) benzyl alcohol in deionized water. Control rats receive diluents. The treatment protocol consists of a single injection of SU5416 (20 mg/kg) at the beginning of the 6 week experiment. The animals are exposed to chronic hypoxia (simulated altitude of 5000 m in a nitrogen dilution chamber) for 4 weeks; thereafter the animals are kept at the altitude of Richmond (sea level) for another 2 weeks. We specifically chose not to use the monocrotaline model, as it was recently shown to be associated with myocarditis<sup>26</sup>.

#### *Pulmonary artery banding*

In male Sprague-Dawley rats weighing 200g anesthesia is induced and maintained by isoflurane inhalation (5% and 2%, respectively, in oxygen-enriched room air). After intubation, the animals

are mechanically ventilated with the use of a volume-controlled respirator. Positive end-expiratory pressure is maintained at 4 cmH<sub>2</sub>O. A left thoracotomy is performed, and the pulmonary artery is carefully dissected free from the aorta. A silk thread is positioned under the pulmonary artery, and an 18-gauge needle is placed alongside the pulmonary artery. A suture is tied tightly around the needle, and the needle is rapidly removed to produce a fixed constricted opening in the lumen equal to the diameter of the needle. The combination of a fixed banding around the pulmonary artery and animal growth results in a pressure gradient of about 50 mmHg (see figure e1) and a marked increased RV afterload. After the banding, the thorax is closed in layers, and postoperative pain relief is obtained by applying buprenorphine (15µg/kg s.c.).

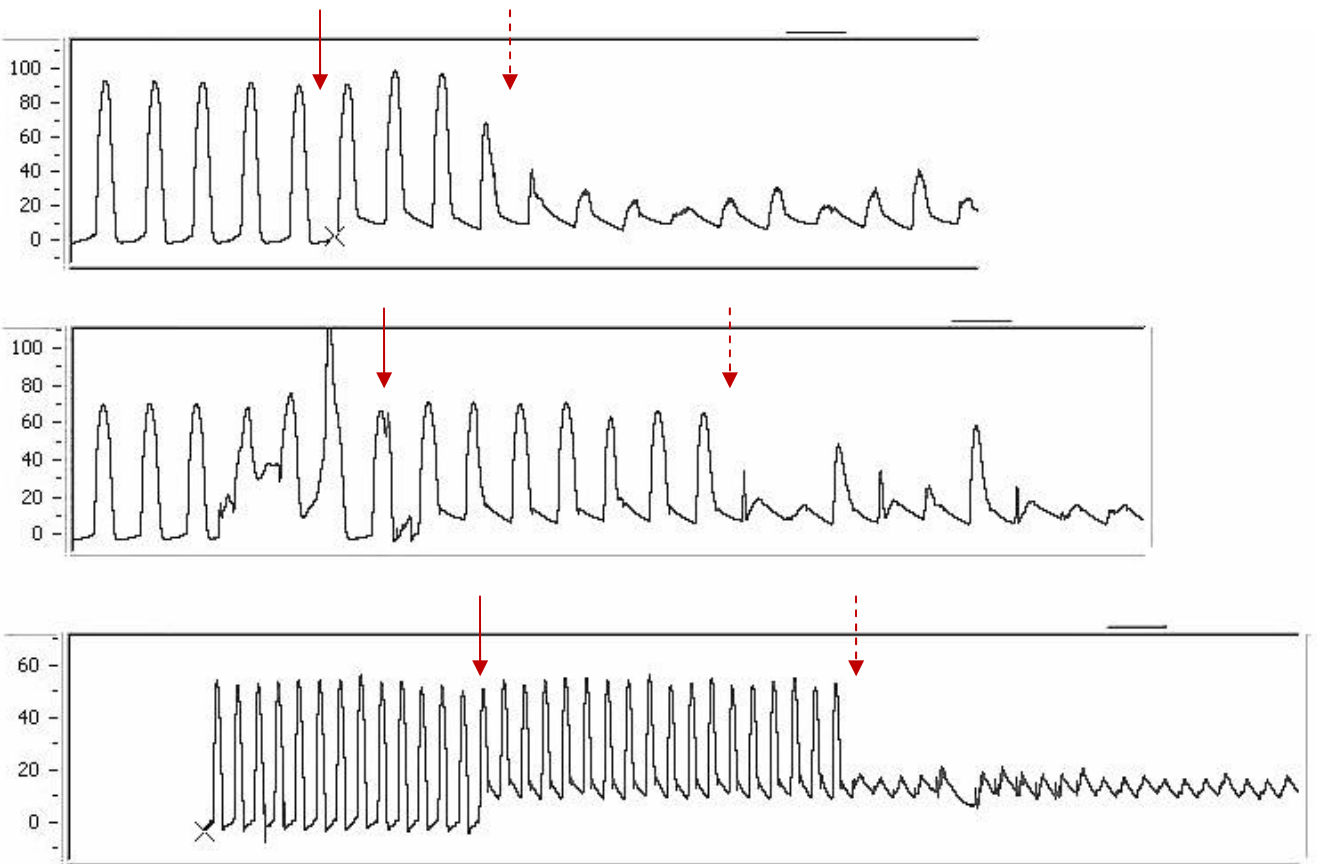


**Figure e1** *Three examples of pressure tracings during the transition of the catheter from right ventricle into the pulmonary artery pressure and beyond the pulmonary artery band. The x-axes (time) have been adjusted for optimal appreciation of the catheter maneuvers. The solid angles show the passage of the pulmonary valve, the dashed arrows show the passing of the stenosis. Pressure gradients determined in stable recordings of at least 30 seconds show an average systolic pulmonary artery pressure gradient of 54 mmHg and an average mean arterial pressure gradient of 17 mmHg over the pulmonary artery stenosis.*

### *Echocardiography*

Doppler echocardiography is performed using the Vevo770 imaging system (VisualSonics, Toronto, Canada) after superficial anesthesia with ketamine/xylazine. The rats are placed in the supine position, and ECG limb electrodes are attached. The chest is carefully shaved, and ultrasound gel is used on the thorax to optimize visibility during the exam. A 30-MHz probe is used to obtain two-dimensional, M-mode and Doppler imaging from a parasternal short-axis view. Measurements are made of RV inner diameter, RV free wall thickness and septal thickness in diastole and systole; pulmonary artery velocity time index and pulmonary artery diameter are also obtained.

### *Hemodynamic measurements*

Hemodynamic measurements are made using the Powerlab system (AD Instruments, Colorado Springs, CO). The rats are anesthetized with isoflurane, intubated and placed in a supine position. Fluid filled polyethylene catheters (PE50) are placed into the carotid artery (for measurements of systemic blood pressure and/or blood sampling) and jugular vein (for i.v.

administrations and/or blood sampling). Subsequently, a median sternotomy is performed, the pericardium opened and a 4.5 mm conductance catheter (Millar Instruments, Houston, TX) is introduced into the RV for measurements of RV pressure volume loops and pulmonary artery pressures (proximal and distal of the PA band, if applicable). After data acquisition, the animals are exsanguinated and tissues are harvested. In separate groups (same experimental conditions) and using the same anesthesia, intubation and catheterization techniques, cardiac output is measured by thermodilution. Saline ( $\pm 12^{\circ}\text{C}$ ) is injected via the jugular catheter (advanced into the right atrium) and the change in temperature is measured in the aorta using a thermocouple (advanced via the carotid catheter). These animals are also used for lectin injections (see below). Data analysis is performed using GraphPad and PVAN software (AD Instruments, Colorado Springs, CO).

### *Microvascular Imaging*

Rats previously anesthetized and instrumented for cardiac output measurements are heparinized using 1000 IU/kg of heparin (American Pharmaceutical partners, Schaumburg, IL) to minimize the formation of microthrombi and occlusion of microcirculatory beds. 0.5 mg of Texas-Red conjugated *lycopersicon esculentum* tomato lectin (Vector laboratories, Burlingame, CA) is injected into the jugular vein. Lectin is an N-acetylglucosamine specific effective marker of blood vessels in rodents. After circulation of the lectin for 5 minutes, 3 mg of papaverin is injected i.v. in order to promote maximal dilatation of all available blood vessels. The abdomen is opened and the rat exsanguinated by cutting the inferior vena cava. Arterial access via the carotid artery is used to perfuse-fix the animal tissues in 2% formaldehyde until tissue blanching. After tissue bleaching and clearing following a protocol of Dickee *et al.*<sup>51</sup>, three dimensional

imaging is performed by confocal microscopy of whole mount sections of approximately 30  $\mu\text{m}$  thickness. Images are collected using a Leica TCS-SP2 AOBS confocal laser scanning microscope (Leica Microsystems, Wetzlar, Germany) equipped with a Märzhäuser MCX-2 motorized XY stage (Märzhäuser, Wetzlar, Germany). A 40x (oil) objective lens is used to collect images, with a scan resolution of 1024x1024 pixels, a scan zoom value of 1 (pixel dimensions =  $0.141\mu\text{m}^2$ ) and a step size of  $0.652\mu\text{m}$  through focus. DAPI is illuminated with a 405 nm diode laser and Texas Red is illuminated with a 594 nm HeNe laser. The detector windows are set to 450-500 nm to collect fluorescence emission of DAPI and 600-675 nm to collect the emission of Texas Red. Stacks of confocal images collected through focus are rendered in 3-D using Volocity software (Version 4.3.2, Improvion, Coventry, UK). From these 3-D volume renderings, capillary density is digitally quantified (using Volocity) and expressed as capillary volume percent of total tissue volume in tissue samples of approximately  $1*10^7\mu\text{m}^3$ .

### *Gene expression studies*

Rat RV, LV and lung are snap frozen in liquid nitrogen. The FastRNA® Pro Green Kit (MPBio) is used to isolate total RNA from heart tissue. Using the FastPrep®- 24 instrument, 25mg of tissue is homogenized by Lysing Matrix D in impact-resistant 2ml tubes. Total RNA released into the proprietary, protective RNapro™ Solution is extracted with chloroform and precipitated using ethanol. Total RNA (1  $\mu\text{g}$ ) is reverse transcribed into complimentary DNA (cDNA) using the High-Capacity cDNA Reverse Transcription Kit (Applied Biosystems). First strand cDNA is diluted and RT-QPCR performed using Power SYBR® Green PCR Master Mix (Applied Biosystems) along with murine specific primers. Cycling parameters are:  $95^\circ\text{C}$ , 10 min and 45

cycles of 95°C, 15 sec, 60°C, 1 min. A dissociation profile is generated after each run to verify specificity of amplification. All PCR assays are performed in triplicate. No template controls and no reverse transcriptase controls are included. Automated gene expression analysis is performed using the Comparative Quantitation module of MxPro QPCR Software (Stratagene) to compare the levels of a target gene in test samples relative to a sample of reference (calibrator from untreated cells).

#### *Protein expression studies*

Western blots were performed using standard procedures and commercially available antibodies (HIF-1 $\alpha$ : #3716, Cell Signaling, Danver MA; HO-1: # SPA-896, Stressgen, Ann Arbor, MI; Nrf2: #sc-722, Santa Cruz Biotechnology, Santa Cruz, CA; VEGF: #sc-152 Santa Cruz). HIF-1 $\alpha$  and Nrf2 protein expressions were determined in nuclear extracts, VEGF and HO-1 in tissue lysates.

#### *Immunohistochemistry*

Lung sections are stained with hematoxylin/eosin to evaluate the severity of the pulmonary vascular disease. A quantitative analysis of luminal obstruction is performed by counting at least 200 small pulmonary arteries (outer diameter < 50  $\mu$ m) per lung section from each rat by an investigator who is unaware of the source of the sections. Vessels are assessed for occlusive lesions and scored as: no evidence of neo-intimal formation (open); partial (<50%) luminal occlusion; and full-luminal occlusion (closed). Masson's Trichrome stain is used to assess the degree of fibrosis in transverse cardiac sections. Fibrosis is quantified on digitized images, on

which blue stained tissue areas are expressed as percentage of the total surface area of RV or LV + septum.

#### *Protandim treatment*

In order to explore the effect of upregulation of innate defense mechanisms against oxidative stress, the dietary supplement Protandim (LifeVantage Corp., Littleton, CO, USA) is extracted in 95% ethanol (100mg Protandim per ml ethanol) and diluted 1:3 in PBS for i.p. injections of 1 ml (25mg Protandim extract). Protandim, known to induce superoxide dismutase (SOD) and/or catalase in rodents in vivo, and to decrease lipid peroxidation, consists of the following ratio of ingredients: *B. monniera* (45% bacosides), 150 mg; *S. marianum* (70–80% silymarin), 225 mg; *W. somnifera* powder, 150 mg; green tea, 98% polyphenols and 45% (95)-epigallocatechin-3-gallate, 75 mg; and turmeric (95% curcumin), 75 mg. These five standardized plant extracts are supplied by Nexgen Pharma (Colorado Springs, CO, USA). Injections are given every other day, starting on the day before SU5416 injection and entry into the hypoxia exposure chamber.

#### *Statistical analysis*

Differences between groups were assessed with ANOVA (parametric) and Kruskal-Wallis (non-parametric) tests; Bonferroni's (parametric) and Dunn's (non-parametric) post-hoc tests were used to assess for significant differences between pairs of groups. P-values < 0.05 were considered significant. For reasons of clarity, all data are reported as means ± SEM, unless specified otherwise, even if the differences between groups were tested with a non-parametric test that makes no use of means and standard deviations. 6-8 rats were used per group, unless specified otherwise. Empirically, after many years of working with pulmonary hypertension

models, if significant differences cannot be found in groups of 6-8 animals of this age, gender and strain, than in our experience a larger number of observations will also not yield meaningful differences.

## **Supplemental results and discussion**

### *Animal models for pulmonary hypertension and right heart failure*

Commonly used rodent models for pulmonary hypertension are based on chronic hypoxic exposure or the injection of the plant alkaloid monocrotaline to generate pulmonary hypertension and RV hypertrophy<sup>6</sup>. Whereas hypoxic exposure in rats is associated with muscularization of small pulmonary arteries and a mild degree of pulmonary hypertension, RV failure does not develop. Although the pulmonary artery pressure in the monocrotaline model is not greatly higher than in the chronic hypoxia model, animals develop heart failure and frequently die<sup>24</sup>. It is doubtful whether the monocrotaline model is appropriate to study PAH associated RV failure, since the alkaloid toxin may cause myocarditis and veno-occlusive disease of the liver<sup>25</sup>. The SuHx model simulates human PAH by inducing angioproliferative pulmonary vascular lesions, severe pulmonary hypertension and, ultimately, RV failure<sup>9</sup>.

### *Collagen 1A1 protein expression and Osteopontin-1 mRNA expression as markers of hypertrophy and fibrosis*

Immunohistochemical findings of differences in fibrosis (Trichrome stain) between controls, PAB rats (small, statistically insignificant increase in fibrosis) and SuHx rats (Trichrome stain suggesting severe fibrosis) were confirmed with Western Blots for Collagen 1A1 expression (see

figure e2) and PCR for OPN-1 mRNA (5-fold increase in OPN-1 mRNA in PAB and a 9-fold increase in OPN-1 mRNA in SuHx).

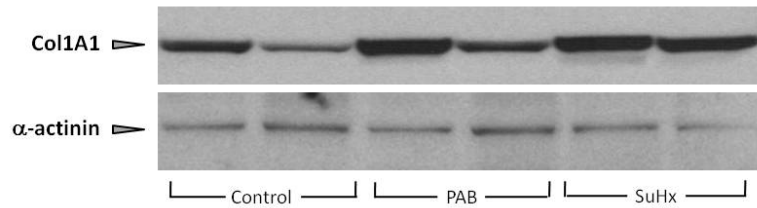


**Figure e2**

*Western Blot for Collagen 1A1 in control rats, rats 6 weeks after surgical banding of the main pulmonary artery and rats exposed to SU5416 and hypoxia.*

OPN-1 expression correlates with the onset of LV hypertrophy and failure<sup>29</sup>, but changes in OPN-1 expression have not been reported in animal models of RV failure. OPN-1 coordinates signals which lead to TGF $\beta$ -1 induced differentiation and migration of myofibroblasts and ECM deposition with the recruitment of macrophages<sup>30</sup>. OPN-1 knock-out mice demonstrate LV dilatation and reduced collagen deposition after myocardial infarction<sup>31</sup>, consistent with the notion that a certain degree of fibrosis may be necessary to adapt to increased myocardial stress. Ultimately, however, cardiac fibrosis interferes with normal contractile physiology and contributes to the development of failure<sup>6</sup>. Whether a moderate degree of cardiac fibrosis is sufficient to explain RV failure is unclear. Mechanical stress and angiotensin II are known inducers of OPN-1 expression<sup>32</sup>, whereas chronic hypoxia is not<sup>33</sup>. We suggest that the increased OPN-1 expression in the SuHx model can be seen as a marker of RV fibrosis

## Supplemental figures and figure legends

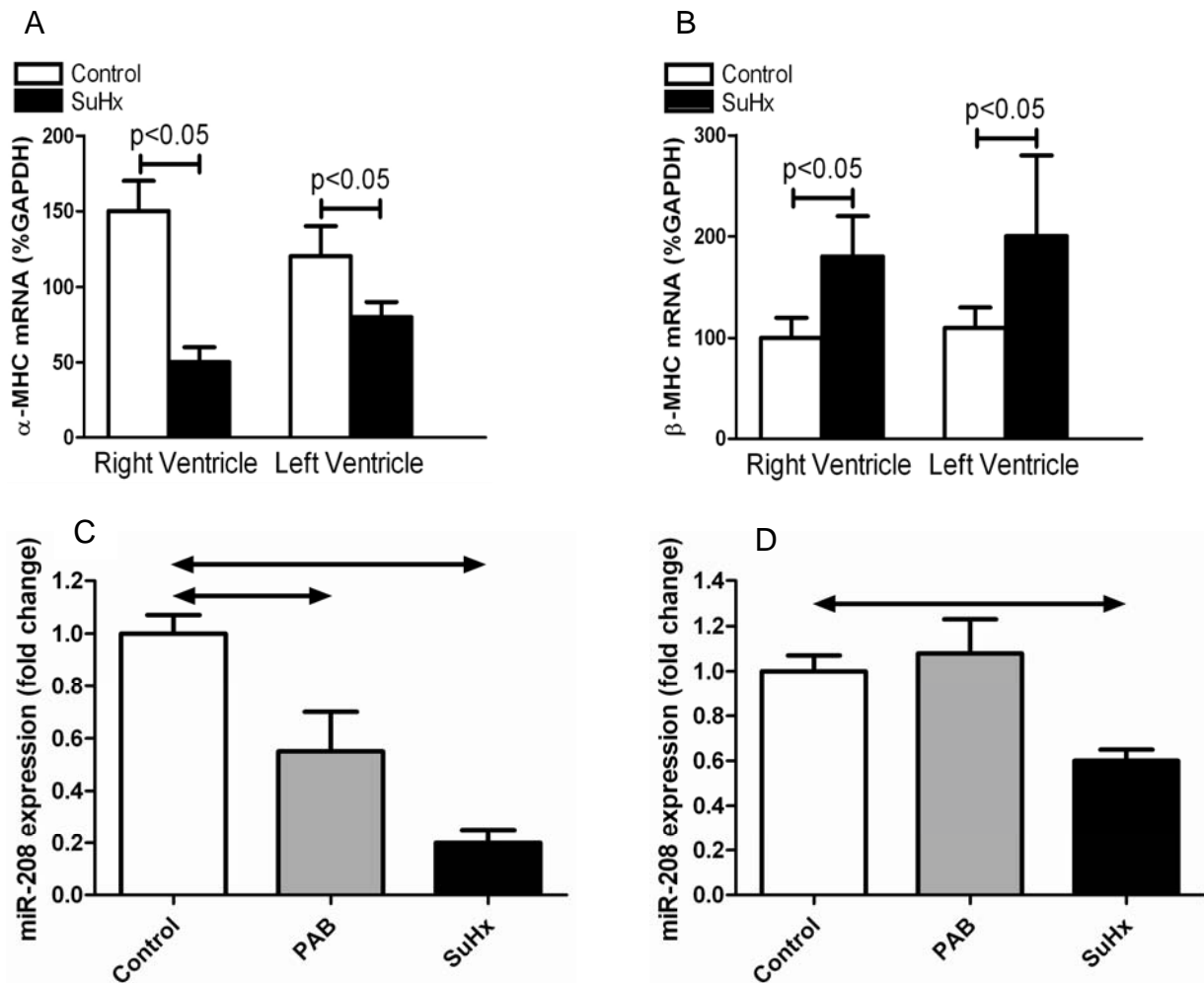


**Figure e3** Fetal gene and micro RNA expression in SuHx and PAB. A unique feature of chronic cardiac stress is a switch in the expression of myosin heavy chain (MHC) genes. Normal hearts typically express  $\alpha$ -MHC, but following stress or injury they switch from the fast contracting  $\alpha$ -MHC to the slower embryonic myosin  $\beta$ -MHC<sup>18</sup>. This switch in MHC isotype expression is part of a general fetal gene reactivation program (together with reactivation of natriuretic peptides), and while fetal gene reactivation was observed in the RV and LV in the SuHx model (Panel A and B), it is also known to occur in states of compensated RV hypertrophy after PAB or chronic hypoxic exposure<sup>19;20</sup>. Interestingly, the gene that encodes  $\alpha$ -MHC gives rise to a cardiac-

*specific miRNA, miR-208. MiR-208 regulates not only cardiac stress responses such as cardiomyocyte hypertrophy and fibrosis, but also plays a central role in regulating the switch from  $\alpha$ -MHC to  $\beta$ -MHC. As seen in panel C, a drastic 80% decrease in miR-208 expression was observed in the RV of rats exposed to SU5416/hypoxia. However, a considerable decrease of 45% in miR-208 expression was also found in the non-failing RV following PAB. MiR-208 expression was preserved in the LV following PAB, and showed only a small decrease in the LV of SuHx animals (panel D).*

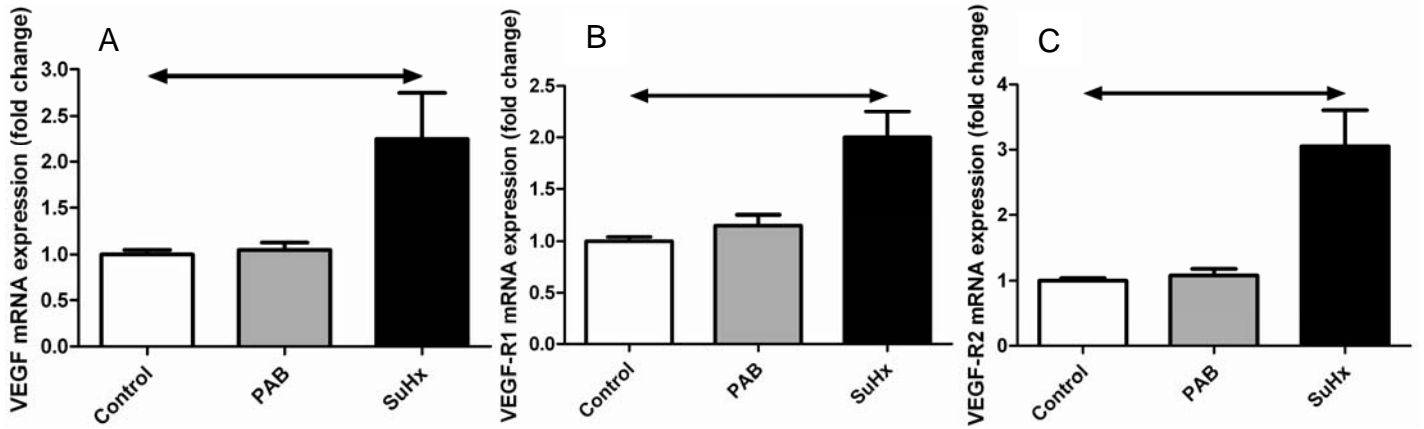


**Figure e4** Left ventricular gene expression of VEGF and VEGF receptors 1 and 2 in the SU5416 hypoxia model (SuHx) and after pulmonary artery banding (PAB). Left ventricular expression of VEGF (panel A), VEGF-R1 (panel B) and VEGF-R2 (panel C) mRNA is significantly increased in SU5416/hypoxia exposed animals but unchanged after PAB.

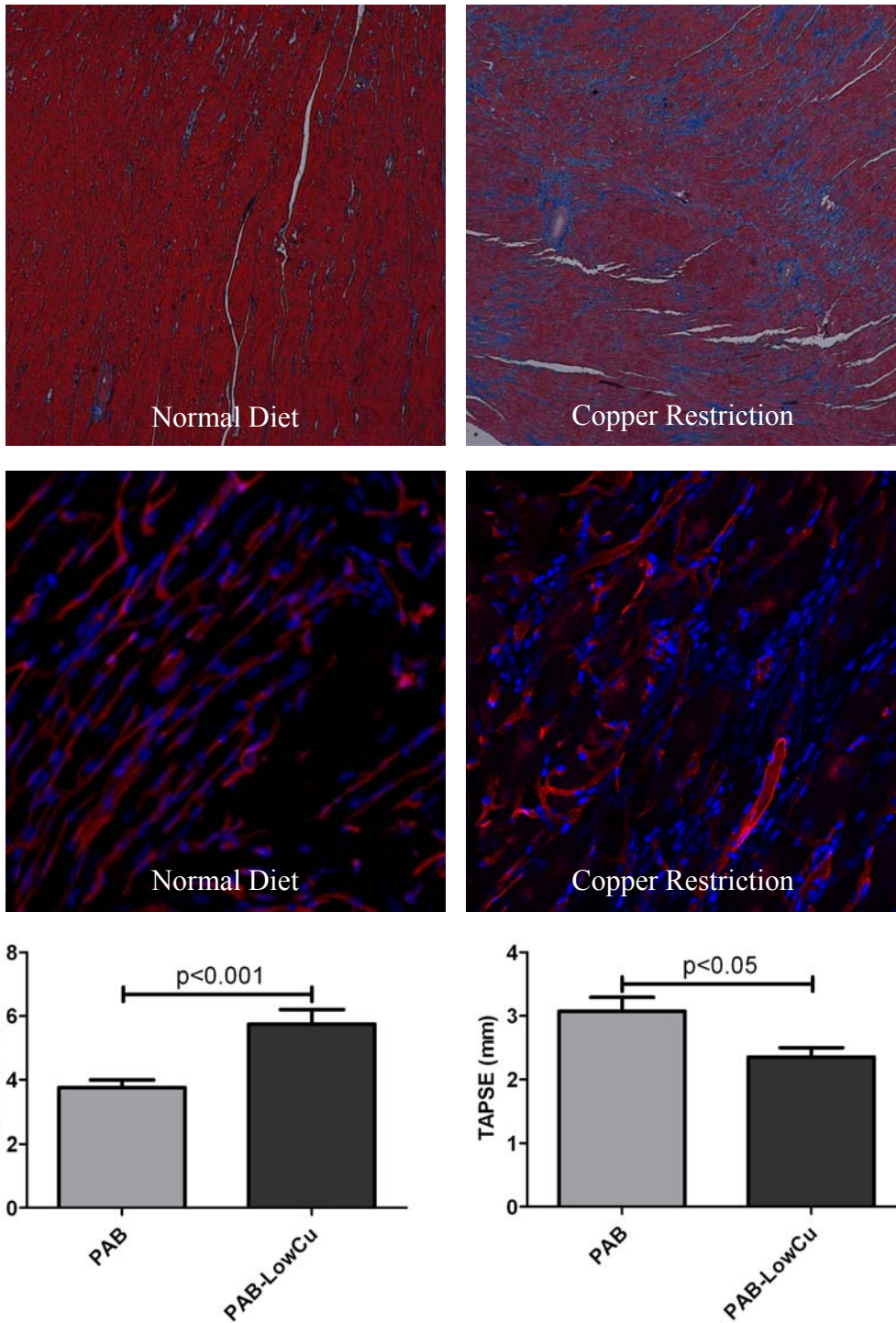


**Figure e5** PAB animals fed with a diet deficient in copper develop RV fibrosis (top panels; Trichrome stain) and capillary rarefaction (middle panels; lectin staining and confocal imaging), along with a depressed RV function on cardiac ultrasound (increased right ventricular inner diameter, RVID, and decreased tricuspid annular plane systolic excursion, TAPSE; lower panels).

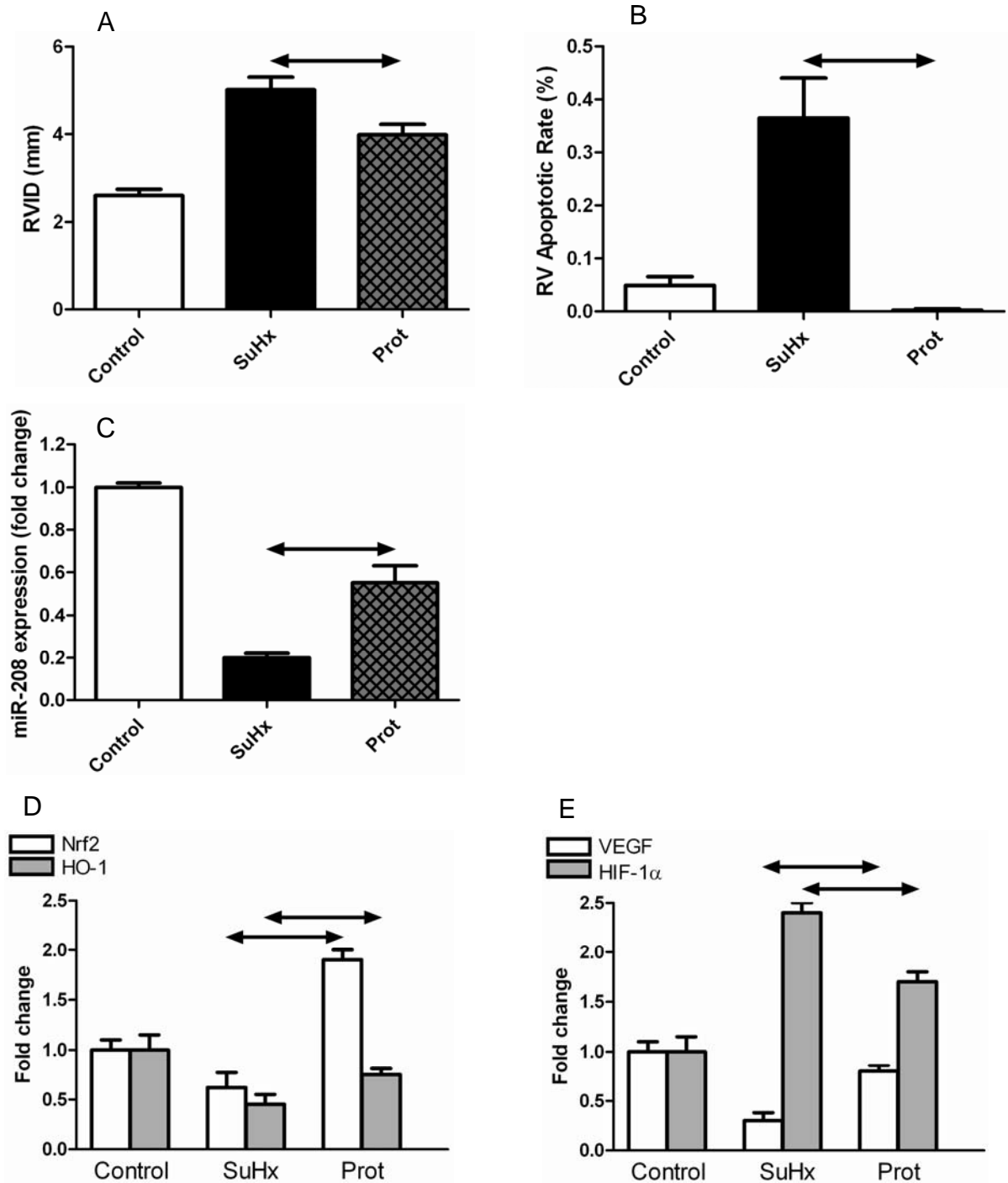


**Figure e6** Protandim (Prot) in the SU5416 hypoxia (SuHx) model attenuates right ventricular (RV) dilatation on cardiac ultrasound (panel A, RVID is RV inner diameter), protects from RV myocardial apoptosis (panel B), attenuates miRNA208 down-regulation (panel C) and prevents hemoxygenase 1 (HO-1, panel D) and VEGF downregulation (panel E), possibly via induction of Nrf2 (panel D).

**Video e1** *Three dimensional confocal imaging of whole mount right ventricular tissue in a model of angio-proliferative pulmonary hypertension associated right heart failure. Capillaries are stained red with Texas Red conjugated tomato lectin, injected intra-vitally. Nuclei are stained blue with DAPI incubation of whole mount samples. See methods for further details. Right ventricular capillaries appear morphologically heterogeneous in the SuHx model and on average there is a lower capillary density in the failing right heart.*

## Chronic Pulmonary Artery Pressure Elevation Is Insufficient to Explain Right Heart Failure

Harm J. Bogaard, Ramesh Natarajan, Scott C. Henderson, Carlin S. Long, Donatas Kraskauskas, Lisa Smithson, Ramzi Ockaili, Joe M. McCord and Norbert F. Voelkel

*Circulation*. 2009;120:1951-1960; originally published online November 2, 2009;  
doi: 10.1161/CIRCULATIONAHA.109.883843

*Circulation* is published by the American Heart Association, 7272 Greenville Avenue, Dallas, TX 75231  
Copyright © 2009 American Heart Association, Inc. All rights reserved.  
Print ISSN: 0009-7322. Online ISSN: 1524-4539

The online version of this article, along with updated information and services, is located on the  
World Wide Web at:

<http://circ.ahajournals.org/content/120/20/1951>

Data Supplement (unedited) at:

<http://circ.ahajournals.org/content/suppl/2009/10/30/CIRCULATIONAHA.109.883843.DC1.html>

**Permissions:** Requests for permissions to reproduce figures, tables, or portions of articles originally published in *Circulation* can be obtained via RightsLink, a service of the Copyright Clearance Center, not the Editorial Office. Once the online version of the published article for which permission is being requested is located, click Request Permissions in the middle column of the Web page under Services. Further information about this process is available in the [Permissions and Rights Question and Answer](#) document.

**Reprints:** Information about reprints can be found online at:  
<http://www.lww.com/reprints>

**Subscriptions:** Information about subscribing to *Circulation* is online at:  
<http://circ.ahajournals.org/subscriptions/>